CoS NWs/Au Hybridized Networks as Efficient Counter Electrodes for Flexible Sensitized Solar Cells

Wenxi Guo, Xiaojia Zhang, Ruomeng Yu, Miaoling Que, Zengming Zhang, Zhiwei Wang, Qilin Hua, Chunfeng Wang, Zhong Lin Wang, and Caofeng Pan**

A newly designed counter electrode (CE) composed of a hybridized structure of Au networks and cobalt sulfide (CoS) nanowire (NW) arrays is presented for flexible dye-sensitized solar cells (DSSCs) and quantum dot-sensitized solar cells (QDSSCs). The sheet resistance of the Au networks electrode is ≈10 Ω sq^{-1} with a transmittance up to 90%. The CoS NWs/Au hybridized networks show excellent electrocatalytic activity and lower charge transfer resistance toward the reduction of both S_x^{2-} ions and I_3^- ions. The hybridized electrode exhibits remarkable mechanical strength and no obvious changes in morphology and sheet resistance even after 500 bending cycles; 3.13% and 4.73% efficiency are obtained by utilizing CoS/Au hybridized networks as CEs in TiO_2 nanotube array (TNAR) based DSSCs and QDSSCs. This work provides a novel approach to fabricate flexible, transparent, conductive, and catalytically active electrodes for QDSSCs and DSSCs and pomotes the development of transparent percolation conductive films for photovoltaics.

1. Introduction

Under the threat of global warming and energy crises, the utilization of green/renewable energy is becoming more and more essential.[1] Thin-film sensitized solar cells (dye-sensitized solar cells (DSSCs) or quantum dot-sensitized solar cells (QDSSCs)) have attracted many attentions due to their ease of roll-to-roll processing, potentially low production costs.[1a,c,2] To date, indium tin oxide (ITO) coated polymer substrates are still the first choice to replace the rigid transparent conductive oxide coated glass substrate to improve the adaptability of DSSCs/QDSCs in transportation, installation, and remote application. Although ITO coated plastics possess good electrical conductivity and optical transmittance properties, this configuration suffers from a number of drawbacks. First, the cost of ITO film is high and indium resource is rare. What is more, ITO is brittle and its conductivity is sensitive to mechanical deformation, preventing it from extensive applications in flexible electronics.[3] Second, the poor chemical stability of ITO film in corrosive/harsh environment significantly restricts its presence in materials synthesizing and devices fabrication processes. To address these problems, many alternative transparent electrode materials including conducting polymers,[4] graphene,[5] carbon nanotube,[6] oxide/metal/oxide multilayer electrodes and metal nanowires (NWs)[3b,7] have been developed to replace ITO film as solutions. Among them, metal NWs or nanotroughs show excellent conductivity and transmittance and they have been applied in touch screens, organic photovoltaic cells (OPVs) and organic light emitting diodes (OLEDs).[7e,8] However, most of the aforementioned studies were focusing on the conductivity and transmittance of the metal network electrodes, but overlooked other features, such as catalytic activity towards the reduction of the ions in electrolytes, chemical stability in corrosive electrolytes and mechanical strength when hybridized with nanomaterials. Therefore, it is necessary to develop newly designed electrodes to meet all these requirements simultaneously for practical applications in flexible QDSSCs/DSSCs.

Here, we developed a back-side illuminated configuration for flexible solar cells composing of TiO_2 nanotube arrays (TNARs)/Ti foil as photoanode and CoS NWs/Au hybridized networks as counter electrode (CE). In this configuration, TNARs possess high specific surface area and Ti foil as a substrate can stand high-temperature (450 °C) processing;[9] highly transparent flexible CE with superior catalytical activity toward the reduction of both S_x^{2-} ions and I_3^-/I^- ions was obtained by selectively synthesizing CoS NWs on Au networks by chemical bath deposition (CBD) method. Furthermore, CoS NWs/Au hybridized networks have been demonstrated exhibiting impressive mechanical property during bending tests. The hybridized electrodes were introduced as CEs for flexible TNAR-based DSSCs and QDSSCs to achieve 3.13% and 4.73% efficiency, respectively.

2. Results and Discussion

2.1. Fabrication of CoS NWs/Au Hybridized Network Electrodes

Figure 1 schematically indicates the fabrication process of CoS NWs/Au hybridized network CE: (1) Polyvinyl alcohol (PVA) nanofiber networks were prepared on the aluminum frame by

Dr. W. Guo, X. Zhang, M. Que, Z. Zhang, Prof. Z. Wang, Q. Hua, C. Wang, Prof. C. Pan
Beijing Institute of Nanoenergy and Nanosystems
Chinese Academy of Sciences
Beijing, China
E-mail: cfpan@binn.cas.cn
R. Yu, Prof. Z. L. Wang
School of Materials Science and Engineering
Georgia Institute of Technology
Atlanta, GA 30332-0245, USA
E-mail: zhong.wang@mse.gatech.edu

DOI: 10.1002/aenm.201500141

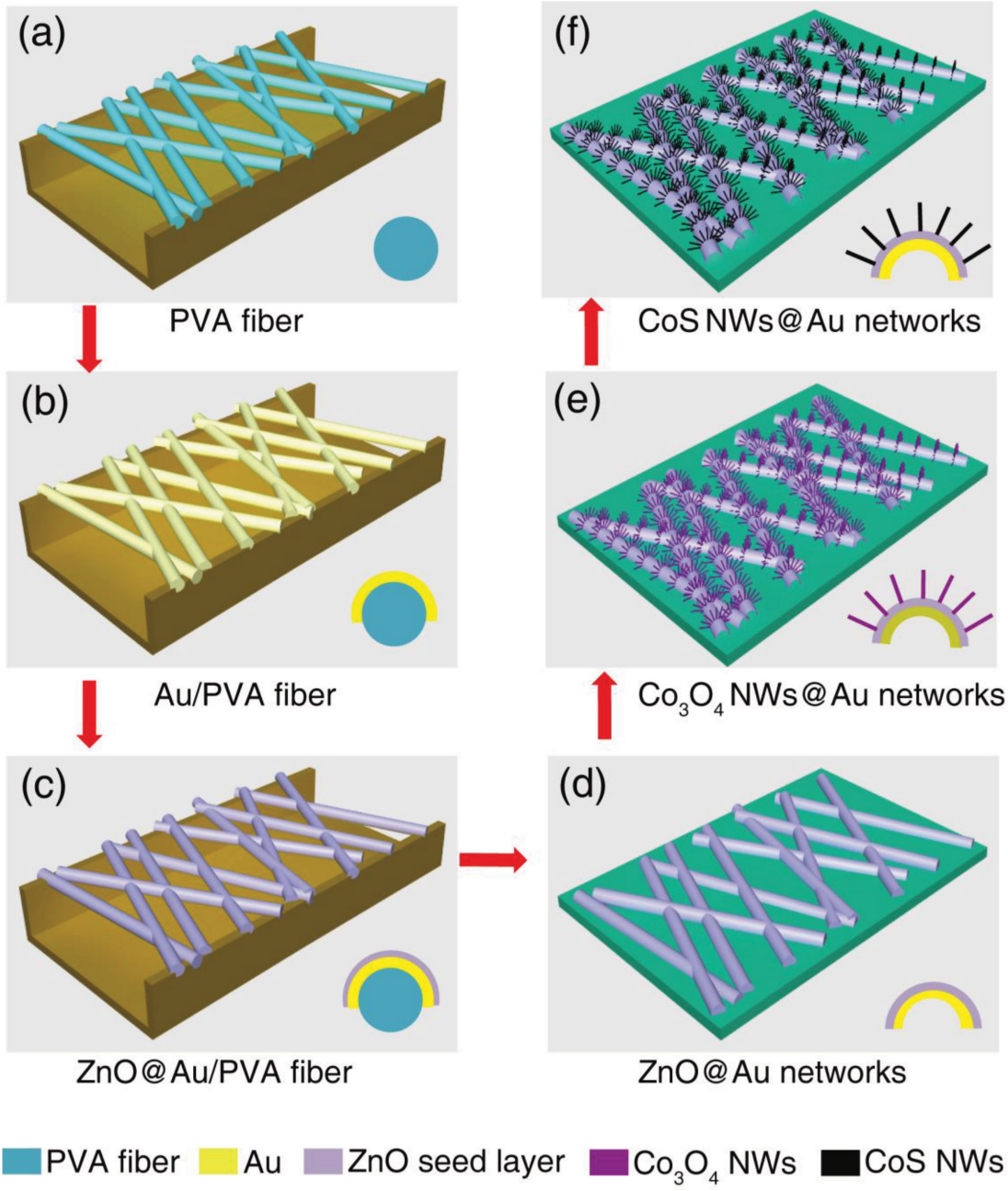

Figure 1. Schematic illustration of the fabrication processes of CoS NWs/Au hybridized networks counter electrode. a) PVA fiber was assembled in networks on an aluminum frame by electrospinning; b,c) Au and ZnO films were subsequently deposited on the PVA surface by magnetron sputtering or thermal evaporation method; d) The hybrid networks were transferred to the PET substrate and the PVA core was dissolved away by subsequently dipping in water; e,f) Co_3O_4 NWs and CoS NWs were subsequently fabricated on the ZnO seeded Au networks by CBD method.

electrospinning as previously reported (Figure 1a);[8d] (2) and (3) Au and ZnO thin films were subsequently deposited on the as-prepared fiber networks using magnetron sputtering (Figure 1b,c); (4) PVA networks were removed by immersing the entire structure in deionized water and hollow structural ZnO/Au networks were transferred onto the polymer substrate (Figure 1d); (5) Co_3O_4 NWs were selectively grown on the ZnO seeded Au networks by CBD method (Figure 1e); (6) Co_3O_4 NWs were transformed into CoS NWs by immersing them into Na_2S solution (Figure 1f).

Optical and scanning electron microscope (SEM) images of the as-prepared CoS NWs/Au hybridized electrodes are presented in **Figure 2**. It is apparent that all the films on the polyethylene terephthalate (PET) substrate are transparent from the optical images shown in Figure 2a. Nanotroughs structured Au networks were derived after removing the PVA nanofibers and transferring the whole structure onto PET substrate as shown in Figure 2b,c. The diameters of the Au nanotroughs can be easily controlled by designing

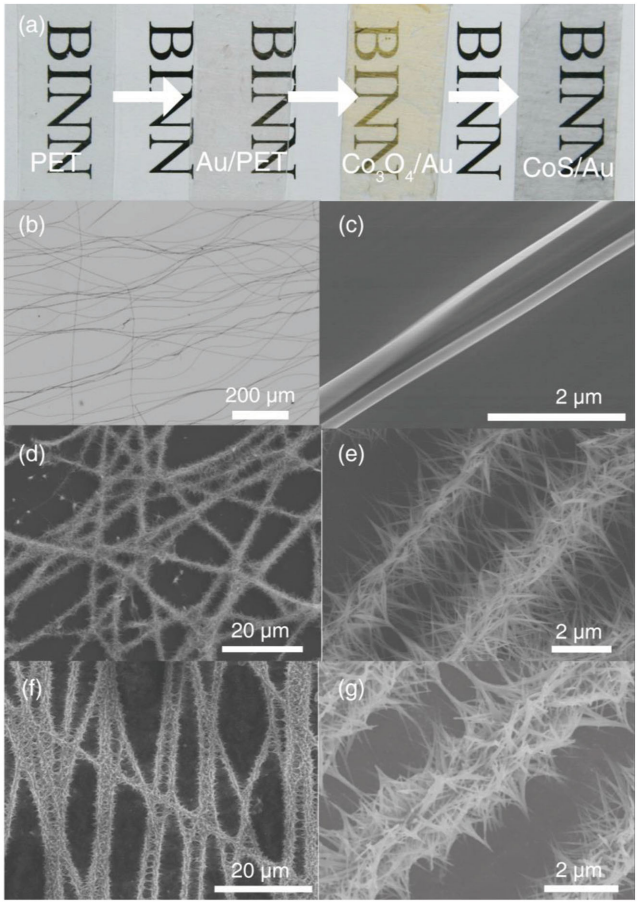

Figure 2. Optical and SEM images of CoS NWs/Au hybridized networks CE. a) Optical images of as-fabricated electrodes in different steps; b,c) optical image and SEM image of as-fabricated Au networks, respectively; d,e) SEM images of as-fabricated Co_3O_4 NWs/Au hybridized networks; f,g) SEM images of as-fabricated CoS NWs/Au hybridized networks.

the geometry of the PVA nanofibers during the electrospinning process. The resistances of the electrodes were mainly controlled by the density of the Au networks, which can be easily controlled by transferred layers. The SEM Images of Au nanotroughs on the PET substrate with different layers are shown in Figure S1 (Supporting Information). Additional transmittance versus sheet resistance performances of Au networks on PET substrates are plotted in Figure 4a,b. It is apparent that with increasing the transmittance of the Au networks films, the sheet resistance increased as expected, and over 98% optical transmittance was achieved with the sheet resistance less than 20 Ω sq^{-1}.

The excellent transmittance and conductivity of the Au networks film suggest its potential to replace ITO as the conductive layer of CEs in flexible solar cells. However, as we know, Au is not an outstanding catalyst for both QDSSCs and DSSCs, the effective way to enhance catalytic ability is to selective construction of high-efficiency catalysts on the networks. As previously reported,[10] CoS exhibited superior catalytic ability towards both polysulfide and triiodide in the applications of QDSSCs and DSSCs. What is more, a recent report on the thin-film solar cells with NW-based transparent electrodes claimed that the light scattering by the NWs can significantly enhance the efficiencies of the device.[11] In these regards, CoS NWs were selectively constructed on the Au networks by following two steps.[10,12] First of all, as a sacrificial template, cobalt oxide NWs were selectively grown on the Au nanotroughs in $CoCl_2$ and urea mixed solution at 90 °C for 3 h. As can be observed from the digital photograph, there is almost no obvious changes in the color and light transmittance after growth of the cobalt oxide NWs. Figure 2d,e shows the corresponding SEM images of the as-prepared cobalt oxide NWs/Au networks on the PET substrate, it is apparent that the entire surface of the Au networks was covered by cobalt oxide NWs that are cylindrical in shape with needle-like top facets. The structure and phase of cobalt oxide are confirmed/analyzed by Raman spectrum and X-ray diffraction (XRD) analysis as shown in Figures S2 and S3 (Supporting Information), indicating that the formation of the obtained NWs is Co_3O_4. It is worth to note that the ZnO seed layer on the Au networks plays an important role in selective growth of Co_3O_4 NWs. Figure S4 (Supporting Information) shows the SEM images of Co_3O_4 NWs grown on Au networks electrode with and without ZnO seeds. As can be observed from Figure S4a (Supporting Information), Co_3O_4 NWs preferentially grown on the PET rather than bare Au networks even the concentration of $CoCl_2.6H_2O$ was as high as 0.15 M. However, after deposition of ZnO seeds on Au networks, Co_3O_4 NWs were successfully grown on Au networks, as shown in Figure S4b (Supporting Information). Selective growth of Co_3O_4 NWs on Au networks was achieved by decreasing the concentration of $CoCl_2.6H_2O$ to 10×10^{-3} M, as displayed in Figure S4c (Supporting Information).

Second, the synthesized Co_3O_4 NWs were then used as templates and transformed into cobalt sulfide NWs by reacting with Na_2S aqueous solution. Figure 2f,g shows the surface morphology of the as-prepared CoS samples after immersing the Co_3O_4 NWs into 0.1 M Na_2S aqueous solution at 90 °C for 16 h. The density and basic morphology of the obtained CoS nanorods remain unchanged. A large-scale SEM image in Figure 2g shows the surface morphology of CoS nanorods was much rougher and shows porous nanostructures. It can be observed from the transmission electron microscopy (TEM) and high resolution transmission electron microscopy (HRTEM) images in **Figure 3**a,b that the distances between lattice fringes are 0.25 nm, indicating the (101) plane of CoS (JCPDS 42-0826).[13] The corresponding selected-area electron diffraction (SAED) pattern (inset of Figure 3a) displays several diffraction rings, revealing the polycrystalline phase of CoS NWs. Furthermore, the energy-dispersive X-ray spectra as displayed in Figure 3c confirms that the as-prepared nanostructures are composed of elements Au, Zn and Co and O. Energy dispersive spectrometer (EDS) mapping in Figure S5 (Supporting Information) shows that all the elements are uniformly distributed on the surface of the Au networks, indicating that Co_3O_4 NWs were mostly transformed into CoS NWs while ZnO seeds still remained on the Au networks. Raman spectrum displayed in Figure 3d with sharp peaks at 190, 474, 516, and 679 cm^{-1} further confirmed the formation of CoS phase after reacting with Na_2S solution.[14]

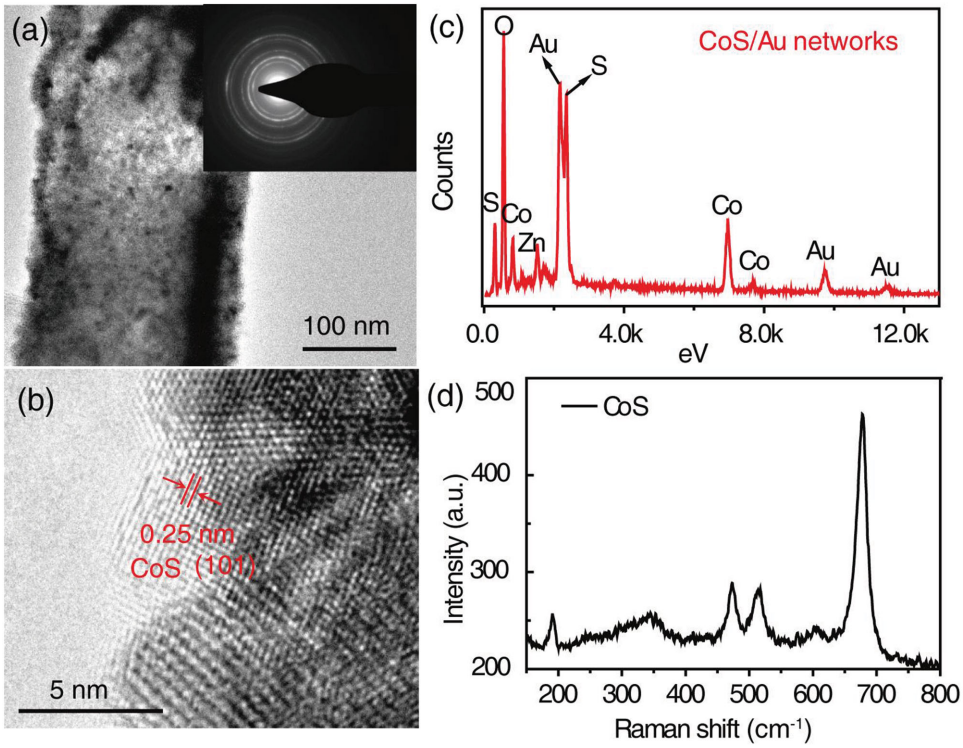

Figure 3. Characterization of CoS NWs/Au hybridized networks CE. a,b) TEM and HRTEM images of the CoS NW grown on the Au nanotrough networks by CBD method, respectively, the inset in (a) is the corresponding SAED pattern; c,d) EDS and Raman spectrum of as-fabricated CoS NWs/Au hybridized networks.

2.2. Physical and Chemical Properties of CoS NWs/Au Hybridized Network Electrodes

As an electrode for flexible solar cells, the CoS NWs/Au hybridized networks have several outstanding features. First, compared with ITO film, Au networks possess excellent optoelectronic performances (**Figure 4**a,b) which are the basis for fabrication of flexible solar cells. Considering that Au is a noble metal, cost-effective passivation coated Cu networks have been studied recently to replace noble metals and potentially being applied in sensitized solar cells.[15] Second, Au networks are conductive percolation films and the selectively growth of nanomaterials on them is beneficial to fabricating transparent electrodes. Figure 4c shows the transmittance spectra of the as-prepared networks electrodes in different processes and commercialized transparent conductive films (ITO and fluorinedoped tin oxide (FTO) on glass) scanned from 400 to 2000 nm. Compared with pure Au networks, no obvious decrease in transmittance was observed from Co_3O_4 NWs/Au hybridized structures, while ≈10% reduction of transmittance was derived after transforming Co_3O_4 into CoS NWs in the range of 400–900 nm. In contrast, CoS NWs film grown on the continuous film (ITO/PET substrate) is almost opaque (less than 5% transmittance), as shown in Figure S6 (Supporting Information). Besides, the conductivity (or density) of the Au networks greatly affected the transmittance of the hybridized network electrode as shown in Figure 4d. Under 550 nm light source scanning, the transmittance of both Co_3O_4 NWs and CoS NWs/Au hybridized electrodes increased as increasing the sheet resistances of Au networks, over 87% optical transmittance was achieved with the sheet resistance more than 20 Ω sq^{-1}, the inset of Figure 4d indicates the variation tendency of transmittances as increasing the sheet resistance of Au network substrates (from left to right). Third, CoS NWs/Au hybridized electrode is highly transparent to NIR light and presents a flat spectrum for the entire wavelength range from 400 to 2000 nm as shown in Figure 4c. On the contrary, the transmittance of commercialized ITO and FTO film on glass suffers a sharp decrease in the range of wavelength greater than 1000 nm. Finally, the Au networks electrode and CoS NWs film on networks demonstrated excellent mechanical strength, which was investigated by monitoring the variations of resistance through periodic bending of both the Au electrodes and ITO (as a comparison) with a 3D positioning system (Figure 4e). No obvious degradation in electrical conductivity was observed for Au networks after 500 bending cycles, while severe degradation was derived in ITO films after several bending. Furthermore, CoS NWs synthesized on the Au networks show better mechanical strength than those grown on continuous films as shown in Figure 4f,g. It is apparent that CoS NWs film on ITO/PET substrate (Figure 4g) partially peeled off with obvious cracks on the surface after bending due to the poor bonding and large surface tension; while no obvious changes in surface morphology was observed for the CoS NWs/Au hybridized electrode after 500 bending cycles (Figure 4f). Owing to the largely reduced size, the NWs/nanotrough hybrid structure exhibit extremely high elasticity that allows large

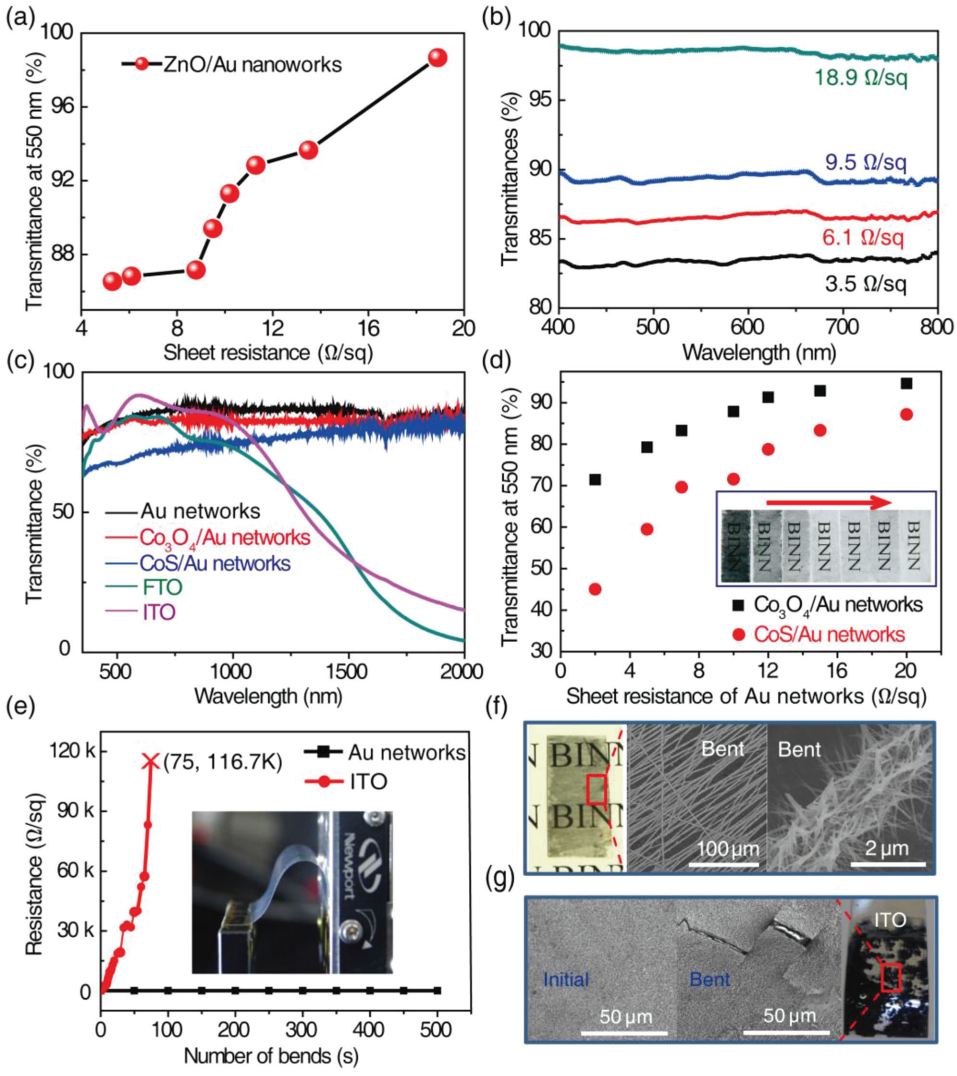

Figure 4. The transmittance and mechanical strength tests of CoS NWs/Au hybridized networks CEs. a) Sheet resistance versus optical transmission (at 550 nm) of Au networks; b) UV–vis spectra of Au networks on PET substrates; and c) the transmittance spectra of the as-prepared network electrodes and commercialized transparent conductive film (ITO and FTO on glass) scanned from 400 to 2000 nm. d) Sheet resistance of Au networks versus optical transmission (at 550 nm) for corresponding Co_3O_4 NWs/Au and CoS NWs/Au hybridized networks, inset is optical image of corresponding seven CoS NWs/Au hybridized network electrodes (the transmittance and sheet resistance increase from left to right); e) variations in resistance of an Au network electrode and an ITO electrode on PET film as a function of the number of bending cycles; the bending tests of f) the CoS NWs/Au hybridized networks and g) CoS NWs/ITO film, the SEM images show the morphology of CoS NWs/Au hybridized networks film and CoS NWs/ITO film after 500 time bending tests, respectively.

degrees of mechanical deformation without cracking or fracture, while thin film can easily generate cracks after applying even smaller strain. As a result, the surface tension of the NWs film on nanotrough is much smaller than that on flexible flat substrate as reported previously.[8d,16]

To evaluate the catalytic activity of the CoS NWs/Au hybridized electrode, cyclic voltammetry (CV) and the electrochemical impedance spectroscopy (EIS) measurements were performed in polysulfide and triiodide electrolyte, respectively. **Figure 5**a displays the CV measurements for symmetrical cells based on Pt, Au, and CoS NWs/Au hybridized network electrodes in polysulfide electrolyte, respectively. During regeneration on the surface of CE, the oxidized species S_x^{2-} gains electrons and is reduced to S^{2-}. In this regard, the current densities at the reduction potential range of CoS NWs/Au networks (Figure 5a, blue lines) were remarkably larger than Pt and Au networks electrodes, suggesting CoS NWs possess higher catalytic activity for S_x^{2-} reduction. Subsequently, electrocatalytic activity of the CEs were further evaluated by EIS measurements, and the Nyquist impedance plots of these symmetrical cells (Figure 5b) indicate that the CoS NWs/Au hybridized electrodes exhibit the smallest R_{ct} of 62.2 Ω cm^2 compared to that of Au (702.6 Ω cm^2) and Co_3O_4 NWs/Au electrodes (357.1 Ω cm^2), confirming the tendency of the reduction current in CV measurements. Similarly, an excellent electrochemical catalytic activity towards the reduction of I_3^- was also derived from CoS NWs/Au hybridized electrodes as shown in Figures 5c–e. The corresponding CV and EIS measurements for symmetrical cells based on Au,

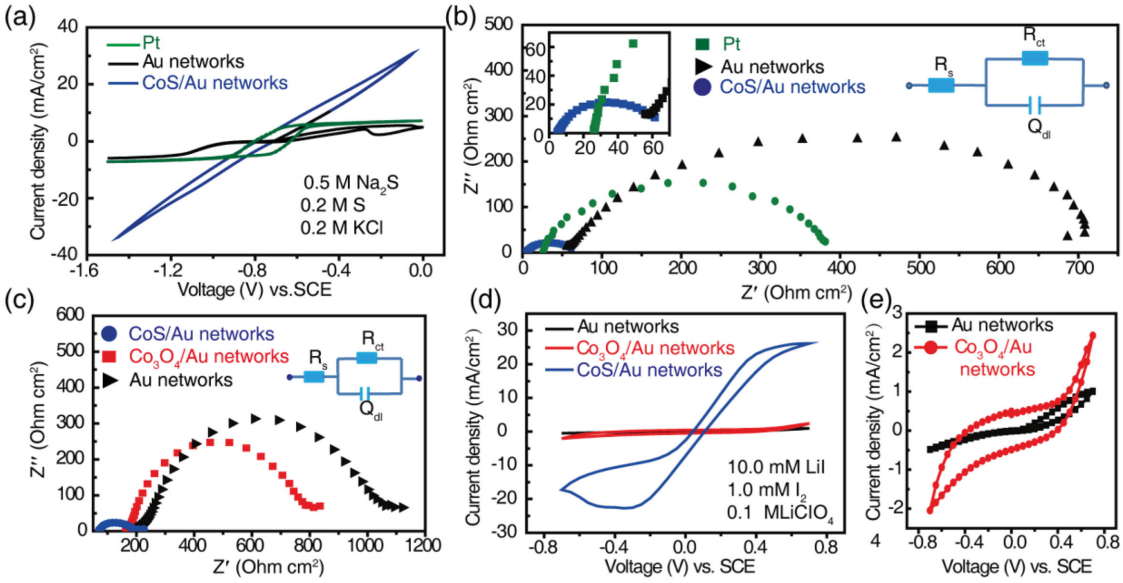

Figure 5. a) Cyclic voltammetric plots and b) Nyquist plots of QDSSCs with Pt, Au networks, and CoS NWs/Au networks as CEs, respectively, the inset in (b) depicts the expanded range of the low value region and the corresponding equivalent circuit; c) Nyquist plots and d,e) cyclic voltammetric plots of DSSCs with Au networks, Co_3O_4 NWs/Au networks and CoS NWs/Au networks as CEs, respectively, the inset in (c) is the corresponding equivalent circuit.

Co_3O_4 NWs/Au and CoS NWs/Au hybridized electrodes in triiodide electrolyte obviously indicate that CoS NWs/Au networks exhibit the highest electrochemical catalytic activity compared with Au and Co_3O_4 NWs/Au electrodes for I_3^- reduction. These electrochemical measurements suggest that the CoS NWs/Au network electrodes are potentially alternative to Pt as the CEs both in QDSSCs and DSSCs.

2.3. Performance of DSSCs and QDSSCs

Figure 6a represents a digital photograph and the corresponding schematic structure of a flexible sensitized solar cell, in which the highly ordered TNARs were employed as photoanode materials, as shown in Figure 6b. Photocurrent density–voltage (*J–V*) curves of QDSSCs based on Au, Pt, and CoS NWs/Au hybridized

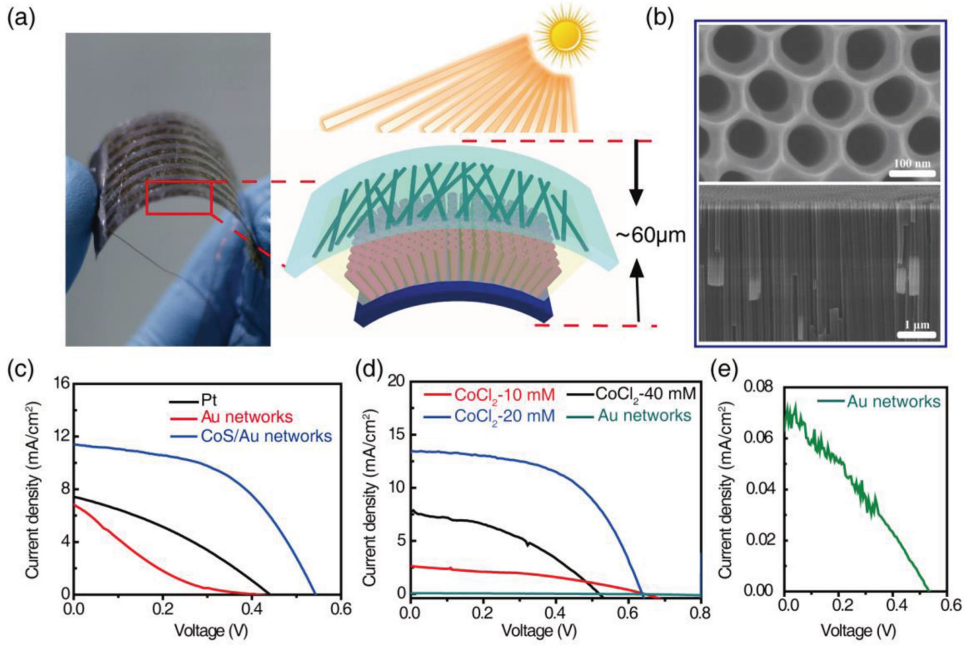

Figure 6. Photovoltaic performances of the QDSSCs and DSSCs. a) A digital photograph of a module and the corresponding schematic structure of flexible TNARs-based sensitized solar cells; b) SEM images of the as-fabricated highly ordered TNARs on Ti foil; c) *J–V* characteristics of QDSSCs with Pt, Au networks and CoS NWs/Au networks as CEs. d,e) *J–V* characteristics of DSSCs with Au networks and CoS NWs/Au networks as CEs.

Table 1. Photovoltaic parameters of the flexible QDSSCs based on different CEs.

Sample	J_{SC} [mA cm^{-2}]	V_{oc} [V]	PCE [%]	FF
Pt	7.42	0.44	1.08	0.33
Au networks	6.72	0.41	0.44	0.16
CoS NWs/Au networks	11.40	0.54	3.13	0.51

electrodes are presented in Figure 6c. To obtained semitransparent Pt CE, Pt nanoparticles were deposited on the FTO glass substrate by means of thermal decomposition (400 °C) as previously reported.[17] The photovoltaic parameters are listed in **Table 1**, indicating that the QDSSC with CoS NWs/Au hybridized CE possess a much better cell performance than others, especially for the J_{SC} and fill factor (FF). The significantly enhanced J_{SC} and FF values indicate that the rate of hole recovery at the CoS NWs/Au hybridized electrode–electrolyte interface is more rapid than that at the other two CEs. A 3.13% efficiency was successfully achieved with the CoS NWs/Au hybridized CEs, which is about 1.9 and 6.1 times higher than those of Pt and Au network CE-based QDSSCs, respectively. In additional, as a high-efficiency catalyst for the reduction of I_3^-, CoS NWs/Au hybridized CE demonstrated great potential application in DSSCs as well. Figure 6d,e displays the *J–V* curves for the DSSCs based on Au and three different CoS NWs/Au hybridized networks electrodes synthesized with different initial concentrations of $CoCl_2.6H_2O$ (10, 20, and 40 × 10^{-3} M), respectively. As expected, the performances of all the CoS NWs/Au hybridized electrodes were much better than that of pure Au network electrode. Furthermore, the density of the CoS NWs which was controlled by the initial concentrations of the $CoCl_2.6H_2O$ would greatly affect the cell's performance. As can be seen from the photovoltaic parameters in **Table 2**, 20 × 10^{-3} M is the optimum concentration for the $CoCl_2$ leading to a 4.73% efficiency of DSSCs. The corresponding incident photon-to-current efficiency (IPCE) spectra as a function of wavelength were shown in Figure S7 (Supporting Information); it is obvious that the IPCE values of all the CoS NWs/Au hybridized electrodes were much better than that of pure Au network electrode. Furthermore, the sample $CoCl_2$-20 × 10^{-3} M has the best performance in IPCE test which totally agrees with the *I–V* results shown in Figure 6d. What is more, in order to investigate the mechanical flexibility of the DSSCs based on CoS NWs/Au hybridized networks electrode, a periodic bending tests were performed. The conversion efficiencies, the FF, and the IPCE spectra of the CoS NW/Au network based DSSC at different bending cycles are shown in Figures S8 and S9 (Supporting Information); it is obvious that the DSSC exhibited remarkable mechanical robustness with only 8% degradation in efficiency after 200 cycles of bending and relaxing. The superior catalytic ability of CoS NWs in DSSCs could be caused by the following: First, NW-based catalytic arrays not only increase surface area of CE films but also accelerate the electron transport; Second, according to the quantum chemistry predictions,[18] the (202) surface of metal sulfide has overpotential behavior in O_2 reduction similar to that observed for platinum electrodes, indicating the special surface structure of metal sulfide benefits the reduction of I^{3-} ions.

Table 2. Photovoltaic parameters of the flexible DSSCs based on different CEs.

Sample	J_{SC} [mA cm^{-2}]	V_{oc} [V]	PCE [%]	FF
$CoCl_2$-40 × 10^{-3} M	7.87	0.52	1.08	0.39
$CoCl_2$-20 × 10^{-3} M	13.35	0.64	4.73	0.55
$CoCl_2$-10 × 10^{-3} M	2.61	0.64	0.64	0.25
Au networks	0.06	0.53	0.01	0.31

3. Conclusion

In summary, we have demonstrated a flexible, transparent, conductive, and catalytically active CE for QDSSCs and DSSCs. Highly interconnected Au networks were fabricated on PET substrate through facile spinning and sputtering with the sheet resistance of less than 10 Ω sq^{-1} and the transmittance up to 90%. CoS NWs were synthesized on the Au networks by two-step CBD method to form the hybridized electrodes with excellent electrocatalytical activity and low charge transfer resistance toward the reduction of both S_x^{2-} ions and I_3^-ions. The hybridized CEs possess impressive mechanical property with no obvious changes in morphology and sheet resistance after 500 bending cycles; 3.13% and 4.73% efficiency were obtained from TNAR-based DSSCs and QDSSCs using CoS NWs/Au hybridized CEs. Such hybrid network electrode could not only replace Pt as CEs in both flexible QDSSCs and DSSCs but also shows potential for applications in wearable electronics.

4. Experimental Section

TNAR Fabrication: TiO_2 nanotube arrays (TNARs) were fabricated on Ti foil by a two-step electrochemically anodization method as reported previously.[12] First of all, a cleaned Ti foil was anodized in ethylene glycol solution containing 0.3 wt% NH_4F and 2 vol% H_2O at 50 V for 9–12 h. Subsequently, the obtained TNRAs on Ti foil were ultrasonically removed in acetone for a few minutes. Then, a second anodization was performed on the same Ti foil under the same circumstances for 2–3 h to produce well-aligned TNARs. The anodized TNARs on the Ti foils were annealed at 450 °C for 2 h in air to form the anatase crystal phase with relatively high crystal purity. To enhance the surface area, a thin TiO_2 nanoparticles layer was deposited on the TNARs/Ti foils electrodes by immersing them in 0.2 M $TiCl_4$ aqueous solution at 70 °C for 30 min, followed annealing treatment was proceeded in muffle furnace at 450 °C for 30 min.

Au Network Fabrication: The transparent Au nanotrough networks were produced using electrospinning and sputtering method as reported previously.[8d] First of all, electrospinning-generated free-standing polymer fibers formed a network in an aluminum frame using water-soluble polymers including 10% PVA (Sigma-Aldrich). Subsequently, a thin layer of Au with thickness of 50–100 nm was deposited on the polymer fiber network by sputtering. The Au networks were transformed to the moistened polymer substrates and then immersing in the deionized water for several hours to remove the polymer template.

CoS NWs/Au Network Fabrication: CoS NWs were fabricated on the Au nanotrough networks by two-step CBD method as previously reported.[10b] First of all, A thin layer of Co_3O_4 (NWs) was grown on the Au networks substrate in an aqueous solution comprised of $CoCl_2{\cdot}6H_2O$ (10 × 10^{-3} M) and urea (0.42 wt%) at 90 °C for 3 h. Then, the as-fabricated Co_3O_4 NWs/Au networks were converted into CoS NWs/Au networks by soaking it in Na_2S aqueous solution (0.01 M) at 90 °C for 12–24 h.

Assembly of the DSSC and QDSSC: For the DSSCs, the TNARs on Ti foil were sensitized with a 0.3×10^{-3} M solution of cis-bis(isothiocyanato)bis(2,2′-bipyridyl-4,4′dicarboxylato)-ruthenium(II) bis(tetrabutylammonium) dye (N-719 as received from Solaronix) in dry ethanol for 24 h. To assemble the QDSSCs, CdS, and CdSe QDs were deposited on the TNARs@Ti foils electrodes by CBD as previously reported.[19] The N719 dye or CdSe/CdS QDs sensitized TNARs@Ti foils were used as the photoanodes and coupled with one of the various electrodes including Pt, CoS NWs networks or Au networks as CE. The aforementioned photoanodes and CEs were assembled together by applying a 25 μm thick hot-melt sealed film as the spacer (SX1170-25; Solaronix Co.). The electrolyte including 0.5 M Na_2S, 0.2 M S, and 0.2 M KCl in a mixture of methanol and deionized water (DIW) (3:7 v/v) and the electrolyte including 0.5 M LiI, 50×10^{-3} M I_2, and 0.5 M 4-tert-butylpyridine in 3-methoxypropionitrile (Fluka) were employed for QDSSCs and DSSCs, respectively.

Characterization: A digital multimeter (Keithley 2100) with a four-point probe was used to measure the films' sheet resistances. The light transmittance of the hybridized electrodes was measured by UV–vis spectroscopy (Shimadzu UV-3600). The optical images were taken by Canon digital camera. The morphology and structure of the prepared hybridized electrodes were examined by scanning electron microscopy (SEM, Hitach 8000) and TEM (F20). The phase identification of the Co_3O_4 NWs/Au networks hybridized electrodes were conducted by XRD using a PANalytical X'Pert PRO diffractometer. Cyclic voltammetric (CV) measurements were performed using an Autolab electrochemical workstation in conventional three-electrode system at a scan rate of 50 mV s^{-1}: One of the various CEs were used as the working electrode, a Pt foil was used as CE, and a saturated calomel electrode were used as reference electrode, respectively. The methanol-DIW (3:7 v/v) mixed solution containing 0.5 M Na_2S, 0.2 M S, and 0.2 M KCl and the ACN solution containing 10.0×10^{-3} M LiI, 1.0×10^{-3} M I_2, and 0.1 M $LiClO_4$ were used as the electrolyte for CV measurements of QDSSCs and DSSCs, respectively. The EIS was carried out on the symmetric cells to measure charge transfer resistance (R_{ct}) using an autolab model PGSTAT 30 (ECOChemie B.V.) equipped with a Frequency Response Analyzer module (Autolab, Eco-Chemie) under a frequency range from 100 kHz to 0.1 Hz and the corresponding ac amplitude was 10 mV. The equivalent circuit models were used to analyze impedance spectra. *J–V* curves of the obtained QDSSCs and DSSCs were measured under simulated solar light (SOLO22A, CROWTECH) with an air mass (AM) 1.5 filter. The IPCE spectra were measured by a monochromator (Oriel, Model: 74125). To examine mechanical durability, the electrode was bent to a radius of 0.5 cm and released to the initial position in a second.

Supporting Information

Supporting Information is available from the Wiley Online Library or from the author.

Acknowledgements

W.G. and X.Z. contributed equally to this work. The authors are thankful for the support from the "Thousands Talents" program for pioneer researcher and his innovation team, China, President Funding of the Chinese Academy of Sciences, National Natural Science Foundation of China (Grant Nos. 51272238, 21321062, 51432005, and 61405040), the Innovation Talent Project of Henan Province (Grant No. 13HASTIT020), Talent Project of Zhengzhou Univ (ZDGD13001), the Beijing Municipal Science and Technology Commission (Z131100006013004 and Z131100006013005), and Surface Engineering Key Lab of LIPCA.

Received: January 19, 2015
Revised: March 10, 2015
Published online:

[1] a) M. M. Lee, J. Teuscher, T. Miyasaka, T. N. Murakami, H. J. Snaith, *Science* **2012**, *338*, 643; b) C. K. Chan, H. L. Peng, G. Liu, K. McIlwrath, X. F. Zhang, R. A. Huggins, Y. Cui, *Nat. Nanotechnol.* **2008**, *3*, 31; c) B. O'Regan, M. Gratzel, *Nature* **1991**, *353*, 737; d) Z. L. Wang, J. H. Song, *Science* **2006**, *312*, 242.

[2] a) M. Gratzel, *J. Photochem. Photobiol., C* **2003**, *4*, 145; b) Z. S. Yang, C. Y. Chen, C. W. Liu, H. T. Chang, *Chem. Commun.* **2010**, *46*, 5485; c) A. J. Nozik, *Physica E* **2002**, *14*, 115; d) M. Law, L. E. Greene, J. C. Johnson, R. Saykally, P. D. Yang, *Nat. Mater.* **2005**, *4*, 455; e) P. V. Kamat, *J. Phys. Chem. C* **2008**, *112*, 18737; f) S. Ruhle, M. Shalom, A. Zaban, *ChemPhysChem* **2010**, *11*, 2290; g) H. C. Weerasinghe, F. Huang, Y.-B. Cheng, *Nano Energy* **2013**, *2*, 174; h) L. Li, T. Zhai, Y. Bando, D. Golberg, *Nano Energy* **2012**, *1*, 91.

[3] a) D. R. Cairns, R. P. Witte, D. K. Sparacin, S. M. Sachsman, D. C. Paine, G. P. Crawford, R. R. Newton, *Appl. Phys. Lett.* **2000**, *76*, 1425; b) D. S. Hecht, L. B. Hu, G. Irvin, *Adv. Mater.* **2011**, *23*, 1482.

[4] S. Kirchmeyer, K. Reuter, *J. Mater. Chem.* **2005**, *15*, 2077.

[5] a) K. S. Kim, Y. Zhao, H. Jang, S. Y. Lee, J. M. Kim, K. S. Kim, J. H. Ahn, P. Kim, J. Y. Choi, B. H. Hong, *Nature* **2009**, *457*, 706; b) N. O. Weiss, H. L. Zhou, L. Liao, Y. Liu, S. Jiang, Y. Huang, X. F. Duan, *Adv. Mater.* **2012**, *24*, 5782; c) S. Bae, H. Kim, Y. Lee, X. F. Xu, J. S. Park, Y. Zheng, J. Balakrishnan, T. Lei, H. R. Kim, Y. I. Song, Y. J. Kim, K. S. Kim, B. Ozyilmaz, J. H. Ahn, B. H. Hong, S. Iijima, *Nat. Nanotechnol.* **2010**, *5*, 574.

[6] a) B. J. Lee, G. H. Jeong, *Appl. Phys. A-Mater.* **2013**, *110*, 29; b) M. Zhang, S. L. Fang, A. A. Zakhidov, S. B. Lee, A. E. Aliev, C. D. Williams, K. R. Atkinson, R. H. Baughman, *Science* **2005**, *309*, 1215.

[7] a) S. De, T. M. Higgins, P. E. Lyons, E. M. Doherty, P. N. Nirmalraj, W. J. Blau, J. J. Boland, J. N. Coleman, *ACS Nano* **2009**, *3*, 1767; b) Z. Chen, S. Ye, I. E. Stewart, B. J. Wiley, *ACS Nano* **2014**, *8*, 9673; c) L. B. Hu, H. S. Kim, J. Y. Lee, P. Peumans, Y. Cui, *ACS Nano* **2010**, *4*, 2955; d) E. C. Garnett, W. S. Cai, J. J. Cha, F. Mahmood, S. T. Connor, M. G. Christoforo, Y. Cui, M. D. McGehee, M. L. Brongersma, *Nat. Mater.* **2012**, *11*, 241; e) S. R. Ye, A. R. Rathmell, Z. F. Chen, I. E. Stewart, B. J. Wiley, *Adv. Mater.* **2014**, *26*, 6670; f) C. Y. Yan, X. Wang, M. Q. Cui, J. X. Wang, W. B. Kang, C. Y. Foo, P. S. Lee, *Adv. Energy Mater.* **2014**, *4*; 1301396 g) S. Soltanian, R. Rahmanian, B. Gholamkhass, N. M. Kiasari, F. Ko, P. Servati, *Adv. Energy Mater.* **2013**, *3*, 1332; h) C. H. Lee, R. Pandey, B. Y. Wang, W. K. Choi, D. K. Choi, Y. J. Oh, *Sol. Energy Mater. Sol. Cells* **2015**, *132*, 80.

[8] a) A. Kumar, C. W. Zhou, *ACS Nano* **2010**, *4*, 11; b) C. J. M. Emmott, A. Urbina, J. Nelson, *Sol. Energy Mater. Sol. Cells* **2012**, *97*, 14; c) I. E. Stewart, A. R. Rathmell, L. Yan, S. R. Ye, P. F. Flowers, W. You, B. J. Wiley, *Nanoscale* **2014**, *6*, 5980; d) H. Wu, D. S. Kong, Z. C. Ruan, P. C. Hsu, S. Wang, Z. F. Yu, T. J. Carney, L. B. Hu, S. H. Fan, Y. Cui, *Nat. Nanotechnol.* **2013**, *8*, 421; e) B. Y. Wang, T. H. Yoo, Y. W. Song, D. S. Lim, Y. J. Oh, *ACS Appl. Mater. Interfaces* **2013**, *5*, 4113.

[9] D. Garcia-Alonso, V. Zardetto, A. J. M. Mackus, F. De Rossi, M. A. Verheijen, T. M. Brown, W. M. M. Kessels, M. Creatore, *Adv. Energy Mater.* **2014**, *4*.1300831

[10] a) M. L. Que, W. X. Guo, X. J. Zhang, X. Y. Li, Q. L. Hua, L. Dong, C. F. Pan, *J. Mater. Chem. A* **2014**, *2*, 13661; b) C. W. Kung, H. W. Chen, C. Y. Lin, K. C. Huang, R. Vittal, K. C. Ho, *ACS Nano* **2012**, *6*, 7016.

[11] B. Y. Wang, T. H. Yoo, J. W. Lim, B. I. Sang, D. S. Lim, W. K. Choi, D. K. Hwang, Y. J. Oh, *Small* **2015**, DOI:10.1002/smll.201402161.

[12] W. X. Guo, C. Chen, M. D. Ye, M. Q. Lv, C. J. Lin, *Nanoscale* **2014**, *6*, 3656.

[13] Y. S. Zhu, Y. Xu, Y. D. Hou, Z. X. Ding, X. C. Wang, *Int. J. Hydrogen Energy* **2014**, *39*, 11873.

[14] C. Pichon, N. Millard-Pinard, F. Valdivieso, A. Chevarier, M. Pijolat, P. C. Leverd, *J. Nucl. Mater.* **2007**, *362*, 502.

[15] a) P. C. Hsu, H. Wu, T. J. Carney, M. T. McDowell, Y. Yang, E. C. Garnett, M. Li, L. B. Hu, Y. Cui, *ACS Nano* **2012**, *6*, 5150; b) Z. F. Chen, S. R. Ye, I. E. Stewart, B. J. Wiley, *ACS Nano* **2014**, *8*, 9673.
[16] a) W. X. Guo, F. Zhang, C. J. Lin, Z. L. Wang, *Adv. Mater.* **2012**, *24*, 4761; b) W. X. Guo, C. Xu, X. Wang, S. H. Wang, C. F. Pan, C. J. Lin, Z. L. Wang, *J. Am. Chem. Soc.* **2012**, *134*, 4437; c) W. X. Guo, C. Xu, G. Zhu, C. F. Pan, C. J. Lin, Z. L. Wang, *Nano Energy* **2012**, *1*, 176.
[17] N. T. Q. Hoa, V. D. Dao, H. S. Choi, *J. Mater. Sci.* **2014**, *49*, 4973.
[18] R. A. Sidik, A. B. Anderson, *J. Phys. Chem. B* **2006**, *110*, 936.
[19] Q. X. Zhang, G. P. Chen, Y. Y. Yang, X. Shen, Y. D. Zhang, C. H. Li, R. C. Yu, Y. H. Luo, D. M. Li, Q. B. Meng, *Phys. Chem. Chem. Phys.* **2012**, *14*, 6479.